

Stability of small cationic platinum clusters

Piero Ferrari,^a Klavs Hansen^{b,c}, Peter Lievens^a, and Ewald Janssens^{*a}

Received 00th January 20xx,
Accepted 00th January 20xx

DOI: 10.1039/x0xx00000x

www.rsc.org/

The relative stability of small cationic platinum clusters is investigated by photofragmentation experiments. Mass spectra show a smooth intensity distribution except for a local intensity minimum at Pt_4^+ , revealing an enhanced stability of the platinum tetramer Pt_4^+ . The possibility that radiative cooling competes with statistical fragmentation after photoexcitation is examined and it is shown that clusters in the $N=3-8$ size range do not radiate on the time scale of the experiment. In absence of radiative cooling, the mass spectra of photofragmented clusters can be well explained by dissociation energies computed using density functional theory. The large calculated HOMO-LUMO gap for Pt_4^+ (~ 1.2 eV) is attributed to its high symmetric structure and provides an explanation for the surprisingly low reactivity of this cluster in different gas-phase reactions.

Introduction

The size-dependent thermodynamic stability of small clusters in molecular beams has a long dated history, starting from the discovery of magic sizes in small sodium clusters [1]. Similar to sodium, coinage metal clusters (Cu, Ag, Au) are known for presenting strongly size-dependent stabilities, a behaviour explained by the delocalization of their valence s electron, which form electronic shells that if closed, give stability to the system [2, 3, 4]. Delocalization here is understood as an electron density that covers the entire cluster volume, with a nodal character resembling that of the electron shells of atoms, but with a different level sequence given the different nature of the confining potential, which is closer to nuclear structure. In transition metal (TM) clusters, however, d -electrons are essential in the valence electronic structure, complicating the picture of itinerant electrons. Delocalization of the valence s -electrons can take place, but orbitals derived from these electrons are usually located deep in the density of states [5]. Instead, the frontier orbitals of TM clusters are mainly determined by $d-d$ and $s-d$ interactions [6]. Therefore, their stability patterns are very different from those of single valence element clusters.

The stability of some TM clusters, such as Co_N^+ [7] and Nb_N^+ [8] for example, have been investigated mass spectrometrically, using collision-induced dissociation. The stability patterns were characterized by the dissociation energy of the $\text{TM}_N^+ \rightarrow \text{TM}_{N-1}^+ + \text{TM}$ channel. Important to note is that, because the electronic

structure of these clusters is strongly determined by d -type states, the simplified counting rules of delocalized electrons does not hold [9]. Thus, understanding of their stabilities requires a detailed investigation of each specific cluster size, combining experiments with theoretical calculations. In this work, we centre our attention on the stability of small platinum clusters.

Here, the stability pattern of Pt_N^+ ($N=3-8$) is investigated by a combination of photofragmentation experiments and density functional theory (DFT) calculations. In photofragmentation experiments, a high fluence laser beam excites a cluster distribution and the fragmentation products are analysed by mass spectrometry. Each observed cluster in the fragmentation chain is the product of a larger precursor size and their observed relative intensities contain information about dissociation energies (D_N), thus providing information on size-to-size stability patterns. Fragmentation experiments, with or without photo-excitation, have previously been applied successfully to elucidate the stabilities of different cluster species [10, 11, 12]. In addition, a combination of photofragmentation experiments and DFT calculations have been used to analyse the size-to-size stability of different elemental clusters [13, 14, 15].

Photofragmentation experiments

Pure Pt clusters are produced by pulsed (10 Hz) laser ablation, following the procedure described in detail in Ref. [16]. Briefly, a pulse of He gas (7 bar) cools a plume of Pt material, produced by the ablation of a pure platinum target with the frequency doubled pulse of a Nd:YAG laser ($\lambda=532$ nm), and the mixture is expanded into vacuum. The average size of the resulting cluster distribution can be tuned by changing the production conditions, such as He gas pressure, laser energy and relative timing of helium release and laser pulse. The abundances of cationic clusters as initially produced in the source vary in a smooth way with the cluster size and show a maximal intensity

^aLaboratory of Solid State Physics and Magnetism, KU Leuven, 3001 Leuven, Belgium.

^bCenter for Joint Quantum Studies and Department of Physics, Tianjin University, 300072 Tianjin, China.

^cDepartment of Physics, University of Gothenburg, 41296 Gothenburg, Sweden

* ewald.janssens@kuleuven.be

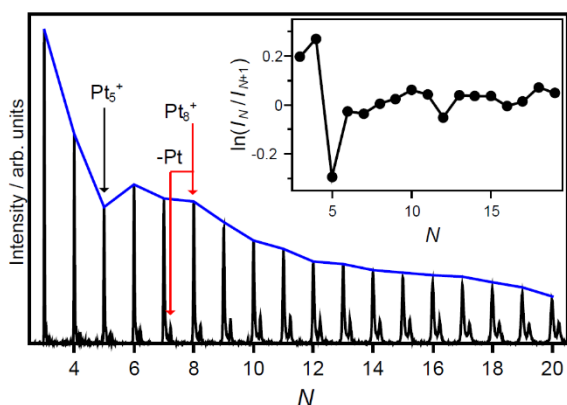


Fig. 1. Mass spectrum of photofragmented Pt_N^+ clusters. The blue continuous line connects the peaks for an easy visualization of the size-to-size intensities. Red arrows indicate, as an example, the $Pt_5^+ \rightarrow Pt_4^+ + Pt$ fragmentation channel. The inset presents the size-dependent logarithm of the ratio in abundances. I_N is calculated as the peak area corresponding to the integrated isotopomeric distribution of Pt_N^+ .

around $N=10$. For the photofragmentation experiments, the initial cationic clusters are electrostatically deflected from the cluster beam. The remaining neutral clusters are exposed to a focused pulse from an excimer F_2 laser ($\lambda=157$ nm), which after a multi-photon absorption process leaves them with a broad energy distribution [17]. This induces fast ionization and fragmentation at the extraction stage of the mass spectrometer. The resulting cluster mass spectrum is recorded in a reflectron time-of-flight mass spectrometer. A detailed description of the experimental setup used here can be found in Ref. [18].

A typical example of a platinum cluster size distribution after ionization and photo-fragmentation is shown in Fig. 1. The spectrum shows a relatively smooth distribution without any strong size-to-size stability variations except for a pronounced minimum at Pt_5^+ . The inset in Fig. 1 quantifies the size-to-size abundances by the quantity $\ln(I_N/I_{N+1})$, with I_N the integrated ion intensity corresponding to the cluster Pt_N^+ . This quantity has its maximum and minimum at Pt_4^+ and Pt_5^+ , respectively,

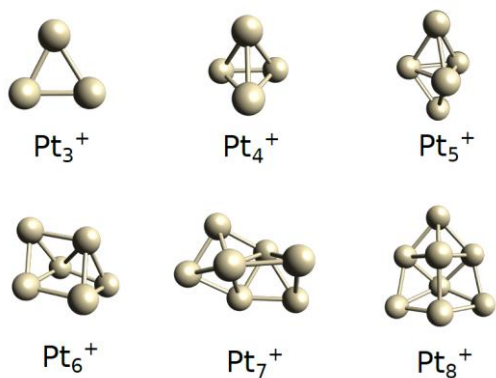


Fig. 3. Density functional theory calculated minimum-energy structures of Pt_N^+ ($N=3-8$) clusters, reoptimized based on the minimum energy structures as determined in Refs. [30, 31, 32].

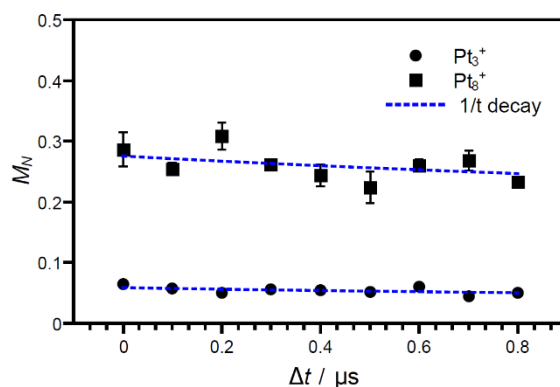


Fig. 2. Metastable fractions (M_N) versus delayed time (Δt) of extraction, corresponding to clusters Pt_3^+ and Pt_8^+ . Eq. (1), assuming a power law decay, is fitted to the data.

whereas above $N=6$ it becomes smooth by the exception of a minor drop at $N=12$.

In between each Pt_N^+ peak in the mass spectrum in Fig. 1, additional peaks of lower intensity can be distinguished. These peaks correspond to metastable fragmentation, which by definition is the delayed fragmentation that occurs in free flight between the extraction and the reflectron stages of the mass spectrometer. Metastable fragments can be distinguished in a mass spectrum because of their slightly different time-of-flight with respect to a prompt fragment, formed in the extraction stage of the mass spectrometer. The flight time of the metastable fragments allows identification of the mass of the clusters produced in the metastable decay [19]. An example is the $Pt_8^+ \rightarrow Pt_7^+ + Pt$ fragmentation channel, which is indicated by red arrows in Fig. 1. Neutral monomer loss is the only fragmentation channel seen for the clusters in this study.

In the absence of a competing decay channels and under excitation conditions leading to broad distributions of energy, clusters have a fragmentation decay rate of $1/t$ [20]. The detected metastable fractions M_N (defined as the intensity in mass spectra of a metastable fragment normalized by the intensity of metastable plus prompt clusters) are therefore proportional to the integral of $1/t$ between the times t_1 and t_2 , representing the moments the clusters leave the extraction and enter the reflection stage of the mass spectrometer, respectively. Thus,

$$M_N = \int_{t_1}^{t_2} A_N \frac{1}{t} dt = A_N \ln\left(\frac{t_2}{t_1}\right), \quad (1)$$

with A_N a proportionality constant. The presence of radiative cooling, which competes with evaporative cooling, quenches the power law decay and thus is recognizable by a faster decay than $1/t$. Radiative cooling has been shown to be significant in carbon based clusters [21, 22, 23, 24], in Si_N^+ [19] and B_N^+ [25], as well as in different kinds of metal clusters: Nb_N^+ [26], Cu_N^+ [27] and Au_N^+ [28]. In order to study the time dependence of the decay, and thus discriminate if radiative cooling is present on the time scale of the experiment, a small time delay Δt is applied between laser excitation and pulsed extraction. By this, flight times are modified to $t_{1,2} = t_{1,2}^{(0)} + \Delta t$ and a plot of M_N

versus Δt allows characterization of the decay. As an example, the metastable fractions versus Δt are presented in Fig. 2 for Pt_3^+ and Pt_8^+ . In both cases, the experimental data is fitted by Eq. (1), using calculated times-of-flight $t_{1,2}^{(0)}$ as input. The satisfactory fittings applying Eq. (1) demonstrate the absence of radiation as a competitive cooling channel for these clusters on the μs time scale of the experiment. This holds for all $N \leq 8$ clusters of this study.

Theoretical calculations

Density functional theory (DFT) calculations on Pt_N^+ in the $N=3-8$ size range were performed with the ORCA 4.0.1 software package [29]. The ground state structures of Pt_3^+ , Pt_4^+ and Pt_5^+ have been determined earlier by a combination of far-infrared multiple photon dissociation spectroscopy and DFT calculations [30]. For Pt_N^+ with $N > 5$ no direct structural information is available and we rely on previous DFT calculations and more indirect structural characterizations. For Pt_6^+ and Pt_7^+ the ground state structures found in Ref. [31] were used. In that work the stretching frequency of adsorbed CO molecules were measured by IR spectroscopy and compared with DFT calculations, finding very good agreement. For $N=8$, the global minimum obtained computationally in Ref. [32] was adopted. All structures were locally re-optimized using the TPSS exchange-correlation functional and Def2-TZVP basis set, as successfully applied in Ref. [31]. 18 electrons were treated explicitly, whereas the other electrons were described by the Stuttgart–Dresden pseudopotentials. In order to check that structural optimization converged to true minima, vibrational frequencies were computed for all cluster sizes.

The lowest-energy structures of Pt_N^+ ($N=3-8$) clusters are presented in Fig. 3. Their size-dependent stability is analysed i) by the second order energy difference ($\Delta_2 E$), comparing the total energy difference between $2 \times \text{Pt}_N^+$ and Pt_{N-1}^+ plus Pt_{N+1}^+ , and ii) by the dissociation energy for neutral monomer evaporation (D_N). Only the neutral monomer evaporation process is considered as dissociation channel, as seen in the experiment. The computed quantities, $\Delta_2 E$ and D_N , are presented in panels (a) and (b) of Fig. 4, respectively.

By comparing the total energy of Pt_N^+ with neighbouring sizes, second order energy differences are a good quantity for analysing relative stabilities [15]. Even though there is no solid framework to directly relate the computed $\Delta_2 E$ values to the intensities in mass spectra, both quantities are usually compared, since they reflect the relative stability of a cluster with respect to its neighbours. Here we see a clear correlation between both, in particular for the predicted higher stability of Pt_4^+ compared to Pt_5^+ . Also in agreement with the experiment, $\Delta_2 E$ shows no significant size-to-size stability variations above $N=5$. Considering the calculated dissociation energies, first we note that, just like in $\Delta_2 E$, a pronounced minimum in D_N is seen at Pt_5^+ , suggesting the relatively stable character of Pt_4^+ . Another quantity obtained from the DFT calculations is the HOMO-LUMO gap. More stable clusters are expected to possess larger HOMO-LUMO gaps, explaining the lower reactivity of these species [33, 34, 35]. Computed HOMO-LUMO gaps, in the

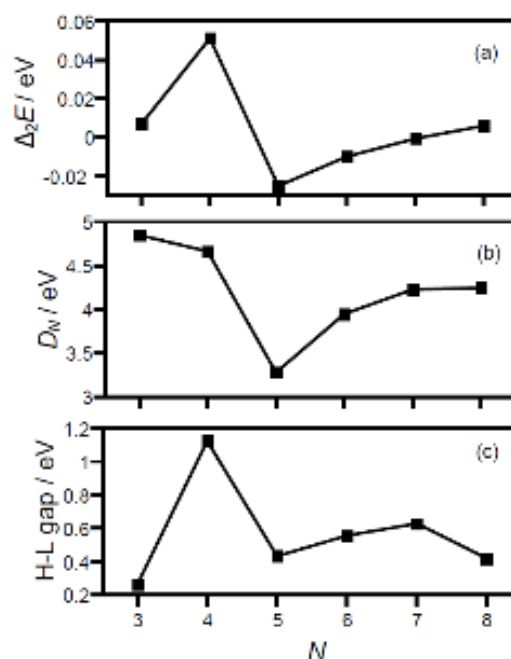


Fig. 4. Computed energetic quantities of Pt_N^+ ($N=3-8$) for the structures shown in Fig. 2: (a) second order differences in energy, $\Delta_2 E$, (b) dissociation energies of monomer evaporation, D_N , and (c) HOMO-LUMO gaps.

$N=3-8$ size range, are presented in Fig. 4c. The largest calculated value is for Pt_4^+ , being approximately 1.1 eV, whereas all other clusters have much smaller gaps between 0.26 and 0.63 eV.

Discussion

In the absence of radiative cooling, intensities in mass spectra can be linked directly with the computed dissociation energies. This is done through Eq. (2), which relates I_N (intensity of the prompt fragments) and D_N (extracted from DFT) [36]:

$$I_N \propto \frac{D_N' + D_{N+1}'}{2} + \frac{s_N}{G_N(t_{1,N})} (D_N' - D_{N+1}') \left(1 + \frac{G_N(t_N)^2}{12s_N^2} \right). \quad (2)$$

In this expression, D_N' is the dissociation energy plus the difference between the caloric curve offsets for reactant and product clusters, which can be estimated as $3/2$ times the Debye frequency of platinum ($\hbar\omega = 0.0194$ eV). s_N is the average of the (microcanonical) heat capacities of reactant and product clusters, which can be set to $3N - 7$. $G_N = \ln(\omega_N t_{1,N})$ is the GSpann parameter, with ω_N a frequency factor. This factor can be calculated by detailed balance theory or from experimental values of platinum vapour pressures [19, 26]. Here we have adopted the second option, using vapour pressure data from Ref. [37]. By doing so, a frequency factor

$\omega_N = 1.508 \cdot 10^{14} N^{2/3}$ is calculated. Fig. 5 shows a comparison of the experimental intensity ratios I_N/I_{N+1} , as extracted from the mass spectrum in Fig. 1, and the calculated ones using Eq. (2). The size-to-size intensity ratio variations are well reproduced by theory, indicating that relative stabilities can indeed be inferred from mass spectra. Therefore, the photofragmentation experiments reveal the absence of strong size-to-size variations in the stability of the platinum clusters, with the exception of the drop at $N=5$.

The absence of size-dependent stability patterns can be understood by analysing the electronic structure of the clusters, which is done with density of state (DOS) plots. Three examples are presented in Fig. 6, for the clusters Pt_3^+ (top), Pt_4^+ (middle) and Pt_5^+ (bottom). The total DOS, in black, is projected onto states with *s*- and *d*-contribution, shown in red and blue, respectively. For the three clusters, the occupied orbitals near the HOMO state are mainly of *d*-character, whereas occupied orbitals of larger *s*-contribution are lower in energy. For the three sizes, one occupied state with the electron density delocalized over the entire cluster and a nodal character resembling the atomic-like 1S orbital is present [2]. Unoccupied states of delocalized character are present as well. They have symmetries corresponding to the atomic-like 1P orbitals: two for the planar Pt_3^+ cluster and three for the three-dimensional Pt_4^+ and Pt_5^+ species. Since the three clusters have the 1S orbital occupied and the 1P shell empty, there are no MOs of delocalized character near the HOMO state. This observation holds for all the calculated clusters.

For the particular case of Pt_4^+ , the relatively higher stability and much larger HOMO-LUMO gap cannot be attributed simply to the filling of electronic shells, as discussed. Comparison of the three DOS plots shown in Fig. 6 reveals a difference between these sizes. In Pt_4^+ , the states composing the DOS have a high degeneracy, due to the high symmetry. All bond lengths in the pyramidal cluster are 2.567 Å. This is particularly clear in the HOMO and LUMO of Pt_4^+ , both composed of three almost degenerate levels, creating a large HOMO-LUMO gap. Similarly, the $1P_{x,y,z}$ atomic-like orbitals are degenerate. In Pt_3^+ and Pt_5^+ , however, the degeneracy is reduced, since the clusters are less symmetric. In Pt_3^+ , there are two shorter bonds of 2.457 Å and a longer one of 2.542 Å, whereas in Pt_5^+ the bond length

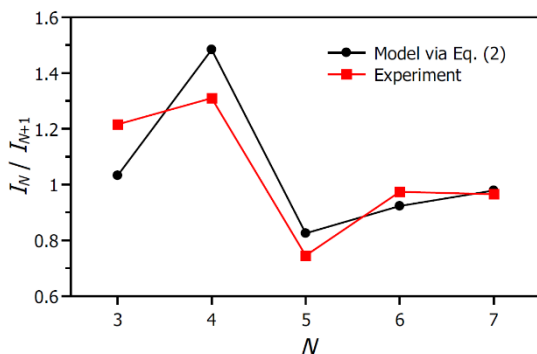


Fig. 5. Comparison of cluster intensity ratios I_N/I_{N+1} obtained mass spectrometrically and based on the computed dissociation energies via Eq. (2).

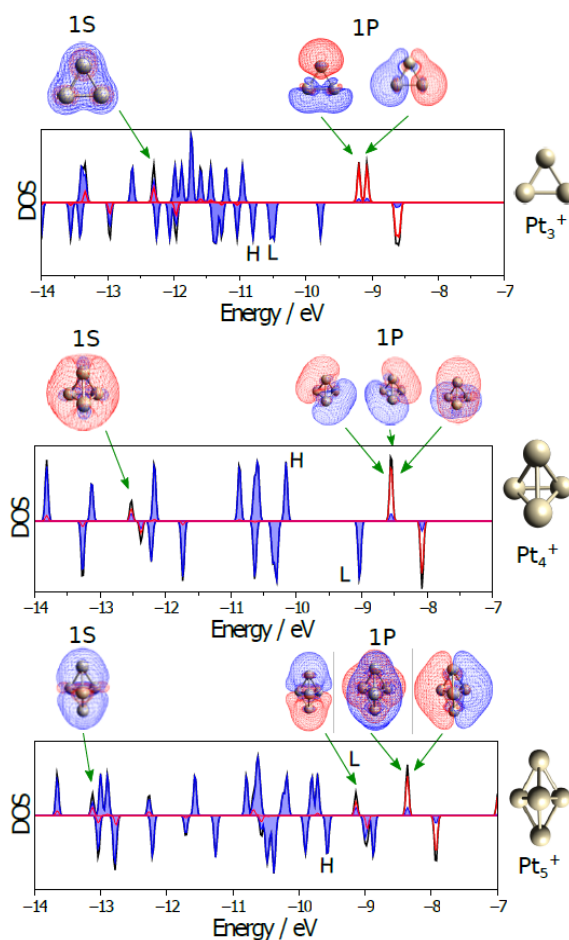


Fig. 6. Density of states (DOS) of Pt_3^+ (top), Pt_4^+ (middle) and Pt_5^+ (bottom). The total DOS (black) is projected onto *s*- and *d*-contributions (red line and blue shading, respectively). The HOMO and LUMO orbitals are labelled with H and L, respectively. At the top of each DOS plot, the MOs of electron density delocalized over the entire cluster are shown. Based on their nodal character, these states are labelled in terms of the eigenstates of the particle confined in a potential well.

between the Pt atoms in the central triangle and the top Pt atom is 2.611 Å, while that between the atoms in the *xy* plane is 2.595 Å. Therefore, the HOMO-LUMO gaps of Pt_3^+ and Pt_5^+ are much smaller than that of Pt_4^+ . This explains the enhanced stability of Pt_4^+ as due to an interplay between the electronic structure and the geometry. In this respect, it would be instructive to compare other charge states for $N=4$, however, the neutral and the anion adopt very different ground state structures [32].

Another interesting observation is the absence of radiative cooling on the time scale of the experiment. In the same experimental setup and under similar experimental conditions, high photon emission rates were measured for other clusters of similar sizes. For example, high and size-dependent radiative rates were measured for small Au_N^+ ($N=6-20$) clusters, with closed-shell species radiating most strongly [28]. Likewise, high rates were measured for B_N^+ ($N=5-20$) [25] and Nb_N^+ ($N=8-22$) [26] clusters, although with a less pronounced size-dependency. Similar experiments have also measured the radiative rates of small Si_N^+ ($N=5-13$), however those have lower values. At this

point is not possible to conclude on the definitive reason for the absence of radiative cooling for the platinum clusters, however it is worth commenting on certain aspects of it. Important is to stress that the performed experiments are only sensitive to radiation taking place on microsecond time scales. Therefore, we cannot exclude the presence of vibrational cooling, which is known to occur at the milliseconds scale [38, 39, 40]. Fast radiative cooling is attributed to the process of recurrent fluorescence [21, 22], which proceeds at a rate determined by three factors: the dissociation energy and size (or heat capacity), essentially determining the effective temperature of the clusters at the moment of photon emission, and the energy of the electronic excited state involved in the photon emission [17]. Recurrent fluorescence requires electronic excited states of sufficiently low energy, thus a possibility to explain the absence of fast photon emission in Pt_N^+ is the absence of such states. A detailed study of the excited states of Pt_N^+ goes beyond the scope of this study. We mention though that in order to explain the very high and size-dependent photon emission rates of Au_N^+ a connection between the pairing of itinerant electrons and low-lying electronic excited states was proposed [28]. For platinum clusters, there are no delocalized MOs near the HOMO state, which in the suggested picture could explain why the platinum clusters do not have low-lying electronic excited states and therefore, fast radiative cooling is absent.

Finally, a comment can be made about previously measured reactivities of cationic platinum clusters. Due to their importance in catalysis, the reactivity of platinum clusters have been the focus of several studies [41, 42, 43, 44, 31, 45]. The reactivity of the small cationic species show a pronounced minimum for Pt_4^+ , particularly in the reaction with methanol. For example, reaction rates for $\text{Pt}_N^+ + \text{CH}_4 \rightarrow \text{Pt}_N\text{CH}_2^+ + \text{H}_2$ have been determined experimentally, giving efficiencies (ratio of the measured rate to the theoretical upper limit calculated for ion-molecule reactions with capture theory) near 1 for $N \leq 8$, except for $N=4$, which has an efficiency as low as 0.02 [43]. This experimental observation has triggered theoretical work to rationalize the low reactivity of the cationic platinum tetramer, focusing mainly on the reaction pathways [46, 47]. An alternative explanation for the low reactivity of Pt_4^+ is the intrinsic thermodynamic stability of this cluster, as shown in the current work. Stable clusters generally have a large HOMO-LUMO gap, as is the case for Pt_4^+ , thus having a low tendency to form chemical bonds with small molecules [48]. This explanation has been invoked in the past to rationalize the low reactivity of certain cluster sizes, such as the low reactivity of Ag_{15}^+ [34] and Al_n^+ ($n = 7, 13$, and 23) [35] towards O_2 , and the reactivity of sodium clusters [33, 49].

Conclusions

In this work, the stability of small positively charged platinum clusters was investigated by combining photofragmentation experiments and density functional theory calculations. The mass spectra of photofragmented clusters revealed a smooth distribution in the size range $N=3-20$, with the exception of an intensity drop at $N=5$, suggesting the absence of size-dependent

stability patterns for the clusters, except for an enhanced relative stability of Pt_4^+ . This is confirmed by energetic quantities calculated for Pt_N^+ in the $N=3-8$ size range. A clear maximum in the second order energy difference is obtained at $N=4$, and a minimum in the monomer dissociation energy for $N=5$. The possibility that radiative cooling competes with fragmentation as a cooling mechanism was also investigated, and it was shown that radiation is absent for all clusters within the time scale of experiment. Furthermore, using the computed dissociation energies, mass spectra abundances were modelled, showing very good agreement with the experimental values. The enhanced stability of Pt_4^+ can be used to explain the previously observed surprisingly low reactivity of this cluster size in the gas-phase.

Conflicts of interest

There are no conflicts to declare.

Acknowledgements

This work was supported by the Research Foundation-Flanders (FWO/G0B41.15N) and the KU Leuven Research Council (C14/18/073). P.F. acknowledges the FWO for a post-doctoral grant.

References

- [1] W. A. De Heer, *Rev. Mod. Phys.*, **1993**, 65, 611.
- [2] H. Häkkinen, *Adv. Phys. X*, **2016**, 1, 467.
- [3] S. Neukermans, E. Janssens, H. Tanaka, R. E. Silverans and P. Lievens, *Phys. Rev. Lett.*, **2003**, 90, 033401.
- [4] V. M. Medel, A. C. Reber, V. Chauhan, P. Sen, A. M. Köster, P. Calaminici and S. N. Khanna, *J. Am. Chem. Soc.*, **2014**, 136, 8229.
- [5] J. T. A. Gilmour, L. Hammerschmidt, J. Schacht and N. Gaston, *J. Chem. Phys.*, **2017**, 147, 154307.
- [6] C. M. Chang and M. Y. Chou, *Phys. Rev. Lett.*, **2004**, 93, 133401.
- [7] D. A. Hales, C. X. Su, L. Lian and P. B. Armentrout, *J. Chem. Phys.*, **1994**, 100, 1049.
- [8] D. A. Hales, L. Lian and P. B. Armentrout, *Int. J. Mass Spectrom. Ion Process.*, **1990**, 102, 269.
- [9] H. Häkkinen, *Chem. Soc. Rev.*, **2008**, 37, 1847.
- [10] J. Pedersen, S. Bjørnholm, J. Borggreen, K. Hansen, T. P. Martin and H. D. Rasmussen, *Nature*, **1991**, 353, 733.
- [11] J. Borggreen, K. Hansen, F. Chandezon, T. Dossing, M. Elhajal and O. Echt, *Phys. Rev. A*, **2000**, 62, 013202.

- [12] N. Veldeman, E. Janssens, K. Hansen, J. De Haeck, R. E. Silverans and P. Lievens, *Faraday Discuss.*, **2008**, 138, 147.
- [13] E. Janssens, H. Tanaka, S. Neukermans, R. Silverans and P. Lievens, *New J. Phys.*, **2003**, 5, 46.1.
- [14] S. Neukermans, E. Janssens, Z. F. Chen, R. E. Silverans, P. v. R. Schleyer and P. Lievens, *Phys. Rev. Lett.*, **2004**, 92, 163401.
- [15] P. Ferrari, H. A. Hussein, C. J. Heard, J. Vanbuel, P. Lievens, R. L. Johnston and E. Janssens, *Phys. Rev. A*, **2018**, 97, 052508.
- [16] M. A. Duncan, *Rev. Sci. Instrum.*, **2012**, 83, 041101.
- [17] K. Hansen, *Statistical Physics of Nanoparticles in the Gas Phase*, Dordrecht, Springer, **2018**.
- [18] P. Ferrari, J. Vanbuel, Y. L. T. Li, E. Janssens and P. Lievens, "Modifications of gas aggregation sources: The double laser ablation source approach," in *Gas aggregation synthesis of nanoparticles*, Weinheim, Wiley-VCH, **2017**, pp. 57-78.
- [19] P. Ferrari, E. Janssens, P. Lievens and K. Hansen, *J. Chem. Phys.*, **2015**, 143, 224313.
- [20] J. U. Andersen, E. Bonderup, K. Hansen, P. Hvelplund, B. Liu, U. V. Pedersen and S. Tomita, *Eur. Phys. J. D*, **2003**, 24, 191.
- [21] Y. Ebara, T. Furukawa, M. J., H. Tanuma, T. Azuma, H. Shiromaru and K. Hansen, *Phys. Rev. Lett.*, **2016**, 117, 133004.
- [22] S. Martin, J. Bernard, B. Brédy, B. Concina, C. Joblin, M. Ji, C. Ortega and L. Chen, *Phys. Rev. Lett.*, **2013**, 110, 063003.
- [23] K. Hansen and E. E. B. Campbell, *J. Chem. Phys.*, **1996**, 104, 5012.
- [24] J. U. Andersen, C. Brink, P. Hvelplund, M. O. Larsson, B. Bech Nielsen and H. Shen, *Phys. Rev. Lett.*, **1996**, 77, 3991.
- [25] P. Ferrari, J. Vanbuel, K. Hansen, P. Lievens, E. Janssens and A. Fielicke, *Phys. Rev. A*, **2018**, 98, 012501.
- [26] K. Hansen, Y. Li, V. Kaydashev and E. Janssens, *J. Chem. Phys.*, **2014**, 141, 024302.
- [27] C. Breitenfeldt, K. Blaum, M. W. Froese, S. George, G. Guzmán-Ramírez, M. Lange, S. Menk, L. Schweikhard and A. Wolf, *Phys. Rev. A*, **2016**, 94, 033407.
- [28] K. Hansen, P. Ferrari, E. Janssens and P. Lievens, *Phys. Rev. A*, **2017**, 96, 022511.
- [29] F. Neese, *Rev.: Comput. Mol. Sci.*, **2012**, 2, 73.
- [30] D. J. Harding, C. Kerpel, D. M. Rayner and A. Fielicke, *J. Chem. Phys.*, **2012**, 136, 211103.
- [31] P. Ferrari, J. Vanbuel, N. Tam, M. T. Nguyen, S. Gewinner, W. Schöllkopf, A. Fielicke and E. Janssens, *Chem. Eur. J.*, **2017**, 33, 4120.
- [32] A. S. Chaves, G. G. Rondina, M. J. Piotrowski, P. Tereshchuk and J. L. F. Da Silva, *J. Phys. Chem. A*, **2014**, 118, 10813.
- [33] T. Lange, H. Göhlich, U. Näher and T. P. Martin, *Chem. Phys. Lett.*, **1992**, 192, 544.
- [34] A. C. Reber, G. U. Gamboa and S. N. Khanna, *J. Phys. Conf. Ser.*, **2013**, 438, 012002.
- [35] R. E. Leuchtner, A. C. Harms and A. W. Castleman Jr., *J. Chem. Phys.*, **1991**, 94, 1093.
- [36] K. Hansen, *Chem. Phys. Lett.*, **2015**, 620, 43.
- [37] J. W. Arblaster, *Platinum Metals Rev.*, **2007**, 51, 130.
- [38] M. Goto, A. E. K. Sundén, H. Shiromaru, J. Matsumoto, H. Tanuma, T. Azuma and K. Hansen, *J. Chem. Phys.*, **2013**, 139, 054306.
- [39] K. Najafian, M. S. Pettersson, B. Dynefors, H. Shiromaru, J. Matsumoto, H. Tanuma, T. Furukawa, T. Azuma and K. Hansen, *J. Chem. Phys.*, **2014**, 140, 104311.
- [40] G. Ito, T. Furukawa, H. Tanuma, J. Matsumoto, H. Shiromaru, T. Majima, M. Goto, T. Azuma and K. Hansen, *Phys. Rev. Lett.*, **2014**, 112, 183001.
- [41] U. Achatz, C. Berg, S. Joos, B. S. Fox, M. K. Beyer, G. Niedner-Schatteburg and V. E. Bondybey, *Chem. Phys. Lett.*, **2000**, 320, 53.
- [42] L. Balteanu, P. Balaj, M. K. Beyer and V. E. Bondybey, *Phys. Chem. Chem. Phys.*, **2004**, 6, 2910.
- [43] C. Adlhart and E. Uggerud, *Chem. Commun.*, **2006**, 0, 2581.
- [44] K. Koszinowski, D. Schroder and H. Schwarz, *J. Phys. Chem. A*, **2003**, 107, 4999.
- [45] C. Adlhart, E. Uggerud, *Chem. Eur. J.* **2007**, 13, 6883.
- [46] L. Lv, Y. Wang, Q. Wang and H. Liu, *J. Phys. Chem. C*, **2010**, 114, 17610.
- [47] F. Xia and Z. Cao, *J. Phys. Chem. A*, **2006**, 110, 10078.
- [48] P. J. Roach, W. H. Woodward, A. W. Castleman Jr., A. C. Reber and S. N. Khanna, *Science*, **2009**, 323, 492.
- [49] A. C. Reber and S. N. Khanna, *Acc. Chem. Res.*, **2017**, 50, 255.